The Potential Predictability in a 14-Year GCM Simulation

WESLEY EBISUZAKI

Climate Analysis Center, National Meteorological Center, Washington, D.C.

(Manuscript received 16 April 1994, in final form 24 April 1995)

ABSTRACT

A 14-yr simulation of a GCM forced by observed SST and sea ice is compared with observations as well as a GCM simulation that used climatological surface conditions. The low frequency (periods > 2 months) behavior in both simulations and observations is examined, and it is found that the anomalous boundary conditions were the cause of much of the low-frequency variability in the simulations. Without the anomalous boundary conditions, the low-frequency spectra was often flat, suggesting that the internal variability was producing a white noise–like spectra. The anomalous boundary conditions were found to be very important in determining the low-frequency behavior of the model. If the future values of the SST and sea ice were known, then the predictability for certain variables could be quite high for low-frequency signals (periods > 8 months). Specific zones showed predictability for low-frequency signals in excess of 70% explained variance. These zones were often related to ENSO, as the Southern Oscillation is the strongest intradecadal phenomenon that is forced by the anomalous boundary conditions. This study gives a lower bound on the variance explained by the anomalous surface forcings.

1. Introduction

Predictability of the atmosphere is determined by both the chaotic nature of the atmosphere and the slowly varying boundary forcings such as SST, sea ice, and solar insolation. The unstable nature of the atmosphere would appear to limit forecasts to a couple of weeks (e.g., Lorenz 1963, 1982) except that the atmosphere supports some low frequency (LF) phenomena such as the quasi-biennial oscillation (QBO), and the boundary conditions have long timescales. The boundary conditions, for example, can be important in forecasting ENSO-related effects, such as drought in Australia or floods in South America. Such forecasts can be quite skillful for leads greater than a month.

Determining the predictability inherent to the anomalous boundary conditions (ABC) can be approached by two methods. One method is to consider the difference between the variance of the atmosphere, which implicitly has ABC, and the hypothetical situation without ABC. Presumably the variance of a system with ABC is larger because the external forcing would tend to increase the variance. The difference of the two variances would be variance that was the result of the ABC and would be "potentially predictable" given the (future) ABC. However, if the ABC modulated the internal variability, then some of this potentially predictable variance would be unpredictable. For example, consider a hypothetical situation where the climate is forced by some process described by a sine wave. The climate signal may look like $\gamma \sin(t) + \epsilon[1 + \alpha \sin(t)]$. Where $\gamma \sin(t)$ is the forced response, ϵ is a random variable, and $\epsilon[1 + \alpha \sin(t)]$ is the internal variability that is modulated by the external forcing. The potentially predictable variance, as defined above, would be $0.5\gamma^2 + 0.5\alpha^2\overline{\epsilon^2}$, where the overbar denotes an average. However, the only predictable part of the climate signal (given ABC) is $\gamma \sin(t)$. Therefore, the potentially predictable variance can include an unpredictable component.

The second approach to potential predictability is as a forecasting problem. How much variance could be explained by simply knowing the ABC. With this approach, the potentially predictable variance is the variance that could actually be predicted given the (future) ABC. Of course, the estimates of this potential predictability can only be a lower bound as techniques (models) are always imperfect.

Chervin (1986) used the first approach to estimate the potential predictability. He used an extended GCM simulation using climatological surface conditions to estimate the variance of the atmosphere without ABC. He then used an F test to find where the observed variance was significantly larger than variance from the GCM simulation, indicating potential predictability. Of course, this approach demands that the model faithfully reproduce the variance of the atmosphere.

Madden and Shea (1978), Madden (1981), and Shea and Madden (1990) also took the first approach. They assumed that the variance consists of two com-

Corresponding author address: Dr. Wesley Ebisuzaki, Climate Analysis Center/NMC5, W/NMC52, Washington, DC 20233.

ponents, the synoptic-scale internal variability and externally forced variability. They estimated synoptic-scale variability from short time series and extrapolated the power spectrum to low frequencies by assuming a white noise extension. This approach is simple; however, it assumes that the low-frequency power spectrum would be white in the absence of ABC and that it can be extrapolated from the power at higher frequencies.

In this paper, we will use the second approach and the second definition of potential predictability. We will use National Meteorological Center's (NMC) global spectral model [Medium-Range Forecast Model (MRF)] to examine how anomalous boundary conditions affect a GCM simulation. There have been previous studies to examine the effects of ABC on MRF forecasts. As part of the DERF 90 project, a comparison of MRF forecasts and simulations was made. The simulations used the same initial conditions as the forecasts but used the observed SST and sea ice unlike the forecasts that damped the SST anomalies with time. Using observed ABC did little to increase the daily skill scores of the simulations (Van den Dool 1994). Mo and Kalnay (1991) and Mo (1992) also examined the effect of the anomalous SST on MRF forecasts. They found that the ABC had a larger effect improving the simulated/predicted monthly means in the tropical regions than in the midlatitudes. Together, these studies suggest that the ABC have a larger effect on the seasonal means than on the daily timescales.

The potential predictability may be a strong function of timescale. For example, one may not expect an SST anomaly lasting 1 month to have the same effect as the same anomaly lasting 1 yr. In this paper, we will try to quantify the variance explained by the ABC and their associated timescales. This will be done by finding the variance common to both the observations and a single GCM simulation forced by observed SST and sea ice. The estimate of potential predictability must be viewed as a lower bound because the estimate could be increased by a better GCM or by using an ensemble of simulations to reduce the internal variability of the estimate.

In this paper, we examine the low-frequency (periods > 2 months) behavior and potential predictability as shown by a 14-yr GCM simulation forced by observed SST and sea ice. This simulation is an extension of the Atmospheric Model Intercomparison Project (AMIP) simulation (see Gates 1992) made by NMC using the MRF. This extended AMIP simulation is compared with observations and another MRF simulation that used climatological boundary conditions.

2. Data sources

For our analysis, we used operational NMC analyses and the output from two GCM simulations. We used monthly means in order to reduce the data requirements. While we had many different fields available, we concentrated on the 200-mb zonal winds. The 200-mb winds have the advantage of being relatively well analyzed because of data from rawindsondes, aircraft, and satellite cloud tracking.

a. AMIP run

We have examined two GCM simulations. The primary simulation is based on NMC's AMIP run (Ebisuzaki and van den Dool 1993). Since we were interested in low frequencies, we extended the original AMIP run by 4 yr. For convenience, we will refer to this extended AMIP simulation simply as the AMIP simulation. The AMIP model had T40 horizontal resolution and 18 sigma layers. The model was run from 1 January 1979 to 1 January 1989 using observed SST and sea ice from the AMIP SST/sea ice dataset, and from 1 January 1989 to 1 January 1993 using the SST and sea ice from R. Reynolds of the Climate Analysis Center (Reynolds and Marsico 1993). The AMIP model was based on the 1992 operational MRF, the model used by NMC to produce the global medium-range forecasts. The AMIP model deviated from it by a lower resolution (T40 versus T126), restoring global dry air mass (unnecessary for operational forecasts), water mass forcing (Qui et al. 1991; Geleyn et al. 1991), and a higher CO_2 concentration (345 versus 330 ppm).

b. NMC10

To examine the importance of ABC in producing low-frequency variability, we used the NMC10 simulation as a control. NMC10 is a T40 MRF simulation using climatological SST, sea ice, snow cover, and soil wetness (van den Dool et al. 1991). The model used in NMC10 is a slightly older version of the MRF than what is used in the AMIP run. The NMC10 model used silhouette orography rather than mean orography, did not restore global atmospheric mass, and did not have water mass forcing.

c. Atmospheric analyses

For comparison with the model-generated data, we also used monthly means of the operational NMC analyses from January 1979 to December 1992 (Dey and Morone 1985), which were archived in the Climate Diagnostics Data Base. We had available the zonal and meridional winds, virtual temperature, and height on standard pressure levels from 1000 to 100 mb. This set of analyses is, unfortunately, inhomogeneous in time. The more recent analyses are of higher quality than older analyses due to the improvements in the NMC analysis system and better use of satellite data. These improvements have caused strong changes in data-poor regions, in particular the Antarctic, and the lowest atmospheric levels. The latter was strongly influenced because the early NMC analysis system ignored much

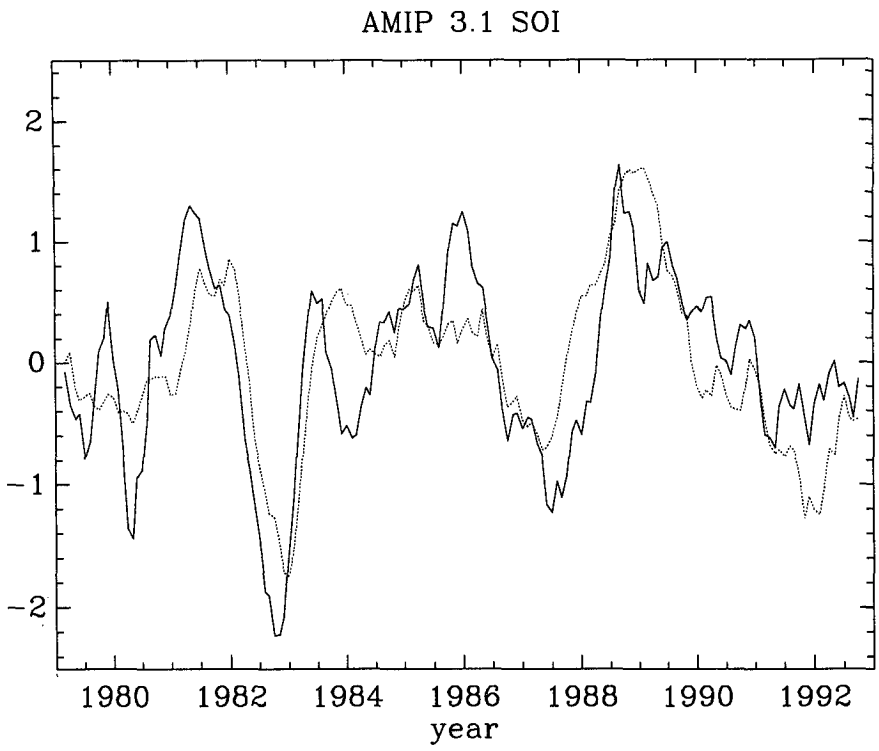

FIG. 1. Southern Oscillation index for AMIP (solid line) and observed (dashed line). Shown are the 5-month running mean of the difference in the normalized sea level pressure between Tahiti and Darwin. Data from 1980 to 1992 were used to calculate the means and standard deviations.

of the surface data (White 1988). Over the years, the vertical resolution, physical parameterizations, and use of surface data have improved (White 1988; White and Caplan 1991), which has resulted in improved surface analyses. However, these improvements have often introduced spurious changes in the surface analyses.

3. AMIP simulation

The AMIP simulation was not perfect. The AMIP model, like all GCMs, has a climatology that differs from the atmosphere's. Many of the model biases resemble those found in earlier studies of the MRF such as White and Caplan (1991). The biases include 1) the easterly bias in the upper-level tropical winds, 2) midlatitude flow tends to be too zonal (T40 resolution), 3) too weak convective activity over the tropical oceans, 4) lower tropical tropospheric cooling, and 5) too much orographic rain. The MRF has its strong points; for example, its Indian monsoon is well simulated considering the model's limited resolution. We account for the imperfections of the model by considering our estimate of the potential predictability to be a lower bound (presumably a perfect model would do better).

The AMIP simulation, however, was able to reproduce some aspects of the Southern Oscillation (SO). We computed a common Southern Oscillation index, a 5-month running mean of the differences in normalized sea level pressure of Tahiti and Darwin where the pressures were normalized by removing the monthly means and by dividing by the standard deviations for the respective month. The correlation was 0.77 between the observed and simulated indices (Fig. 1). Another variable that has been associated with ENSO is the angular momentum (Rosen and Salstein 1983). The simulated 200-mb angular momentum is smaller than the observed because of the easterly bias in the tropical winds; however, the LF anomalies were accurately reproduced (Fig. 2). While the AMIP run was able to reproduce some features of the SO quite well, other features were not well done. For example, the pressure difference between the sea level pressure at Tahiti and Darwin showed that the AMIP run had the correct phase, but the response to El Niño was much too weak (not shown).

4. Potential predictability

One method to find the variance explained by the ABC is to find the anomaly correlation (AC) between the AMIP simulation and observations. Tables 1 and 2 show the AC for selected monthly mean quantities from the 1979–88 subset of the AMIP run (nonextended AMIP simulation). To calculate the AC, the 10-

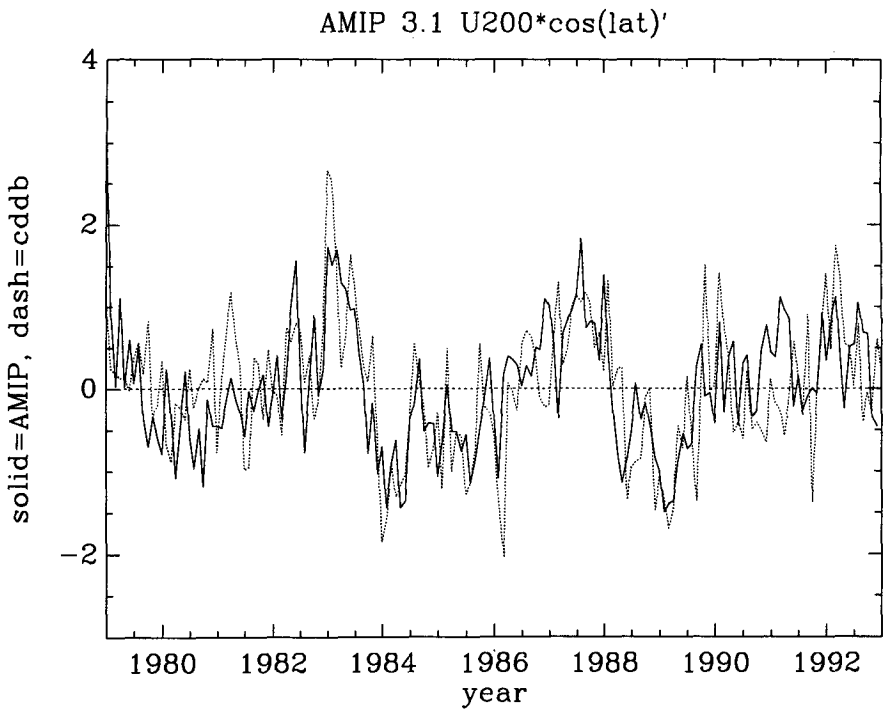

FIG. 2. The 200-mb global average of $U\cdot\cos(\text{lat})$ (m s^{-1}) for AMIP (solid) and observations (dashed) with the annual cycles removed.

yr climatology was removed from the observed monthly means, and the 10-yr model climatology was removed from the model monthly means. The major aspects of the AC tables are 1) more skill in the Tropics, 2) global means are better simulated than horizontal fields, and 3) no usable skill in the midlatitudes for the quantities and domains examined.

The ACs for the 200-mb zonal winds (Table 1), for example, appear to be quite modest. However, the ACs do not take into account that some timescales are more predictable. To examine the potential predictability as a function of timescale, we will calculate the spectral power and coherence.

Consider two finite-length time series $A(t)$ and $B(t)$ that have been decomposed into Fourier modes:

$$A(t) = \text{Re}[\sum_j \tilde{A}(\omega_j) \exp(-i\omega_j t)]$$

$$B(t) = \text{Re}[\sum_j \tilde{B}(\omega_j) \exp(-i\omega_j t)]$$

The spectral power of A is $|\tilde{A}(\omega)|^2$, and coherence is $|\gamma(\omega)|^2$ where

$$\gamma(\omega) = E[\tilde{A}^*(\omega)\tilde{B}(\omega)][E(|\tilde{A}(\omega)|^2]^{-1/2} \times E[|\tilde{B}(\omega)|^2]^{-1/2},$$

and $E(x)$ is the expected value of x.

The coherence $|\gamma|^2$ is similar to the square of the correlation. More detailed explanations can be found in textbooks on spectral analysis such as Otnes and Enochson (1978). Note that some authors have adopted a different terminology and refer to $|\gamma|^2$ as the "square of the coherence."

As a practical matter, the data were preprocessed by removing the annual cycle and a linear trend. Both are common practices in spectral analysis. For the power-spectra calculations, a Bartlett window was used to reduce spectral leakage.

In Fig. 3, we plot the power of the 200-mb angular momentum from observations, the AMIP run, and the

TABLE 1. Anomaly correlation (AC) for monthly averaged U (zonal wind) and Z (geopotential height) for various latitude bands from the NMC AMIP simulation (1979–88).

AC	80°–20°N	20°N–20°S	20°–80°S
U 200 mb	0.04	0.18	0.12
U 850 mb	−0.02	0.16	0.08
Z 200 mb	0.04	0.41	0.08
Z 500 mb	0.00	0.26	0.09

TABLE 2. Anomaly correlation (AC) for various monthly averaged global quantities from the NMC AMIP simulation (1979–88).

AC for global mean	
200 mb ang. momentum	0.64
850 mb ang. momentum	−0.04
200 mb geopotential height	0.50
500 mb geopotential height	0.31

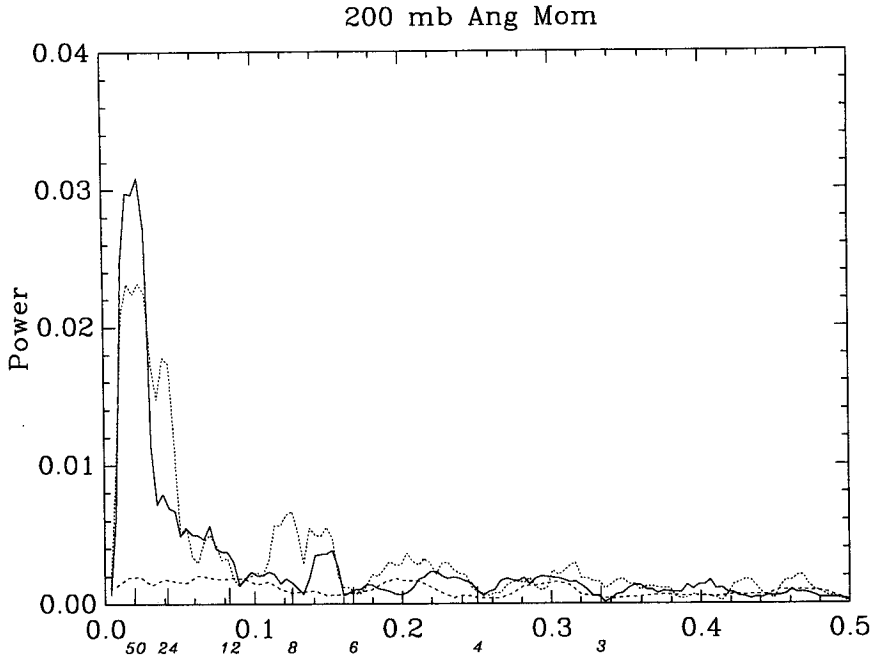

FIG. 3. Power spectra of the 200-mb global average of $U \cdot \cos(\text{lat})$ for the AMIP simulation (1980–92, solid line), observations (1980–92, dashed line), and NMC10 (10-yr, dotted line). Like the following figures, the annual cycle has been removed. The upper abscissa scale is the frequency in mo^{-1}, and the lower scale is the period in months.

NMC10 run (no ABC). In this and all following figures of spectra and coherences, the upper abscissa scale is the frequency in mo^{-1}, and the lower scale is the period in months. We see that without ABC, the power spectrum is extremely deficient in low-frequency variability. This deficiency is not limited to ENSO frequencies, but also extends to periods as short as 7 months. Another feature is that the NMC10 power spectrum resembles white noise, that is, equal power at all resolved frequencies (period $>$ 2 months). The AMIP model and observations show, on the other hand, a strong ENSO peak.

The results shown in Fig. 3 are consistent with the ideas of Madden and Shea (1978), Madden (1981), and Shea and Madden (1990). They assumed that in the absence of ABC, the variance would be forced by the synoptic-scale variability and look white at the low frequencies, much like NMC10's spectrum. (More precisely, the spectrum appears to be the low-frequency limit of a red spectrum.) If we take the previous authors approach, the variance that is the result of the ABC would either be the difference between the observed and white noise variance or the difference between the observed and NMC10's variance. As seen in Fig. 3, the fraction of variance due to the ABC is quite large at ENSO frequencies and very small at high frequencies (periods shorter than 6 months).

Estimating the variance due to ABC by comparing the white noise spectrum to the observed spectrum is valid if the spectrum is white in the absence of ABC. Figure 3 appears to support such an assumption; however, there is a QBO peak (around 24 months) in the observed power spectrum. Since the QBO is thought to be independent of the ABC (Lindzen and Holton 1968), the white noise assumption is immediately suspect, at least for the 200-mb angular momentum. The inability of the AMIP and NMC10 models to simulate a QBO is a failing of perhaps all current GCMs.

Our approach to quantify the potential predictability is by the coherence. The coherence between the observed and simulated angular momentum is quite high for low frequencies (Fig. 4). At 250 mb, the coherence is significant for periods greater than 14 months, reaching values of greater than 0.8 for periods greater than 40 months (i.e., greater than 80% explained variance). The coherence is also significant as low as 800 mb even though the model had less variance in its power spectrum than did observations (not shown). The last notable feature is the poor coherence at 100 mb. The low coherence may have been caused by model deficiencies (being too close to the model top or by poor vertical resolution).

Most of the low-frequency coherences are statistically significant as we can reject the null hypothesis at any prespecified frequency at the 99% confidence, whenever the coherence is 0.26 or greater, and assuming that the data is normally distributed. If we chose the frequency a posteriori, a higher coherence is nec-

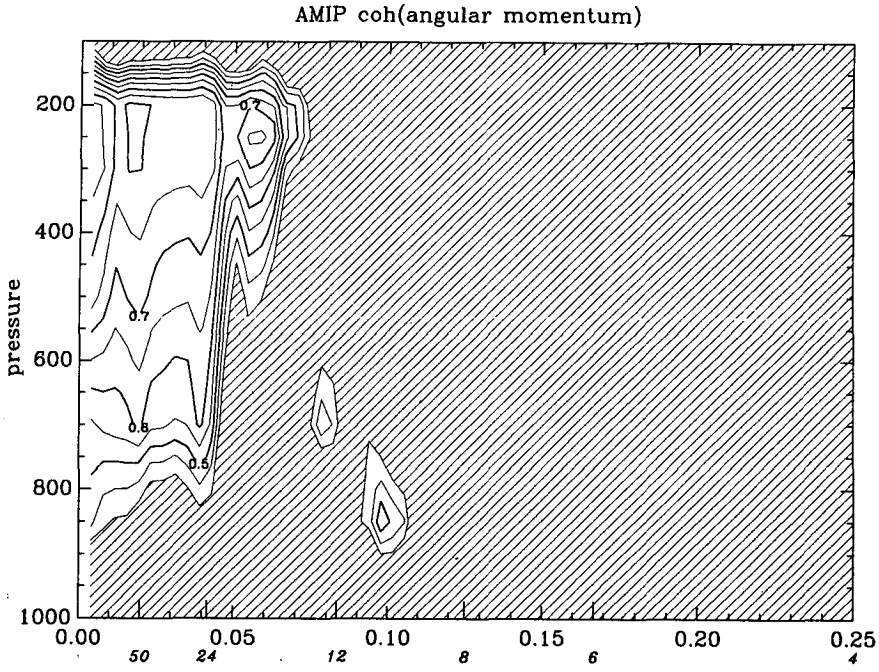

FIG. 4. Coherence between globally averaged $U \cdot \cos(\text{lat})$ from observations and the AMIP simulation (1980–92). The upper abscissa scale is the frequency in mo^{-1}, and the lower scale is the period in months.

essary for statistical significance. Since the Fourier transform determined the power for 128 different frequencies, and the coherence was calculated in bands of 13 different frequencies, the number of degrees of freedom is approximately 10 (128/13). To reject the null hypothesis at the 0.01 level for 10 independent samples, the individual samples should be significant at the 0.001 level. This suggests that the coherence should be above 0.37 for a 99% test. Unfortunately, extreme events in the data (e.g., the 1983 ENSO event) could dominate the statistics, which would make 0.37 an underestimate.

a. Subtropical Pacific winds

The atmosphere has many low-frequency phenomena as can be seen in the power spectra of Pacific winds (Fig. 5). The spectral peak with a period of 60 months is due to ENSO. The peak tropospheric response occurs around 700 mb. The maximum in Fig. 5 (30 months period at 100 mb) is due to the QBO. While the strongest QBO response is in the stratosphere, we see evidence of the QBO as low as 300 mb. Some features in Fig. 5 are artifacts of the analysis scheme. For example, the spectra is not red because the record is too short to resolve the very low frequencies and because the data was initially detrended, which removes some of the LF power. In addition, the annual cycle was removed from the data. The plots of the spectral power do not show zero power at 12 months because the power estimates were smoothed in order to reduce the noise.

The LF power spectra from the AMIP run (Fig. 6) differs from that of the observed winds. First, the AMIP run has no indication of a QBO, a common problem of GCMs. In addition, the simulated ENSO response was weaker in the lower troposphere, peaked at 500 mb rather than at 700 mb, and appears to have a higher frequency. The difference in frequency is not statistically significant because the spectral power estimates have a standard deviation of 20% of the true value, which can shift the frequency of peak power. Some differences in the vertical structure may be due to the vertical distribution of convective heating being poorly simulated as suggested by the changes in this heating, typically found during the first few days of MRF integrations (G. White 1993, personal communication).

Dramatic differences between observations and simulation can be found in the upper troposphere and stratosphere. Above 300 mb, the simulated ENSO response increases in strength with height. The observed spectra, on the other hand, decreases with height above 700 mb. The enhanced upper-level ENSO signal in the simulation may be the result of the easterly bias in the model's tropical winds. Upward propagating tropical waves would normally be trapped by the upper-level westerlies. However, these waves may not be trapped in the model because of its lack of upper-level westerlies or because of the limited vertical resolution in the stratosphere.

The coherence between observed and simulated tropical Pacific winds is above 0.5 (50% explained

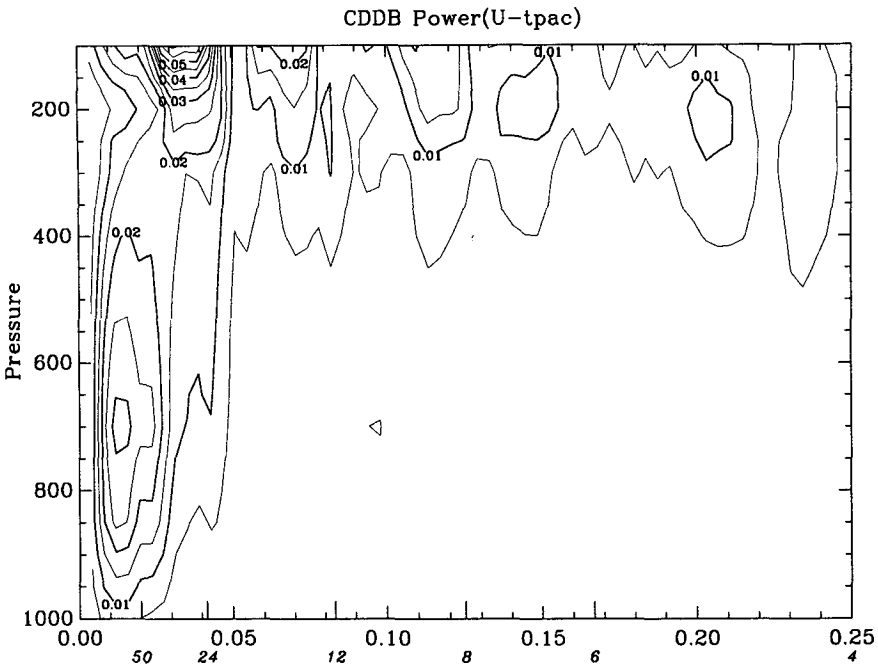

FIG. 5. Power spectra of domain-averaged zonal winds (Pacific). The domain is 30°S–30°N, 120°E–90°W for the period 1980–92. The power spectra were calculated using standard pressure level data. The upper abscissa scale is the frequency in mo^{-1}, and the lower scale is the period in months.

variance) for most of the troposphere for periods greater than 2 yr (Fig. 7). The LF coherence drops above 200 mb. This is probably caused by the AMIP model not being able to predict the QBO and having a very strong stratospheric response at ENSO frequencies. The coherence also shows a region of minor co-

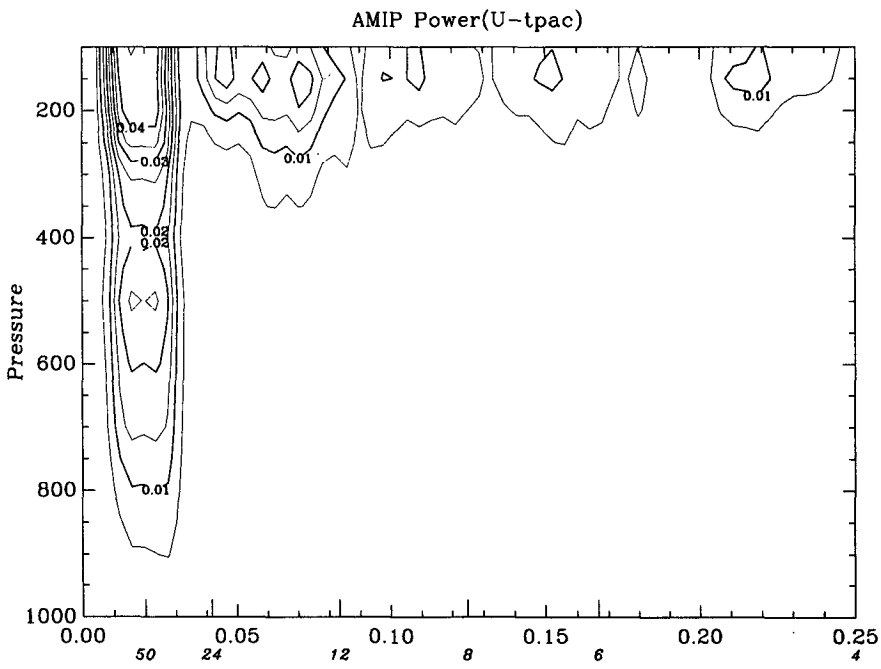

FIG. 6. As in Fig. 5 except the winds from the AMIP run were used.

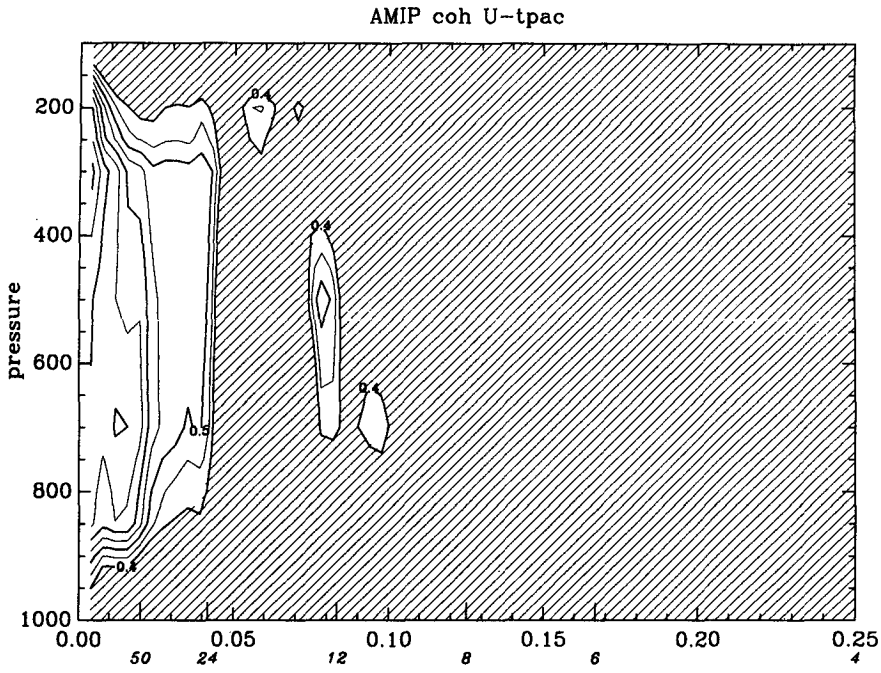

FIG. 7. Coherence between domain-averaged zonal winds (Pacific, 30°S–30°N, 120°E–90°W) from the AMIP simulation and observations (1980–92). The upper abscissa scale is the frequency in mo^{-1}, and the lower scale is the period in months.

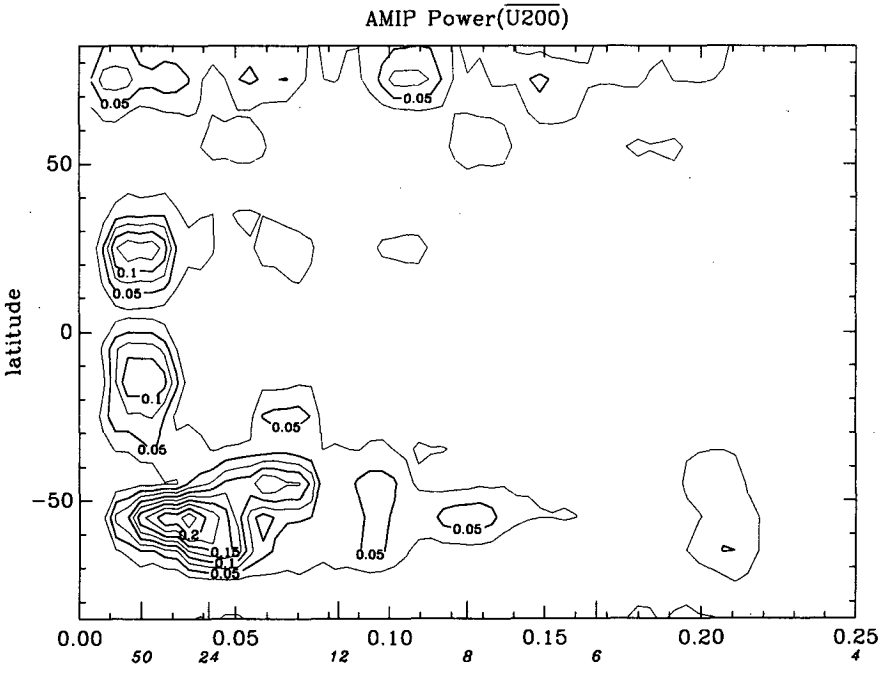

FIG. 8. Power spectra for the 200-mb zonal-mean zonal winds from the AMIP simulation (1980–92). The winds were averaged in 10° latitudinal bands. One standard deviation is 20% of the true value of the spectral power. The upper abscissa scale is the frequency in mo^{-1}, and the lower scale is the period in months.

herence in the midtroposphere at a period of 13 months. Except for this and other few minor regions, the coherence is not significantly different from zero for periods shorter than 20 months.

b. *Zonally averaged U200*

The meridional structure of the LF variability illustrates different mechanisms at work. The AMIP run shows four regions of high variability in the 200-mb zonally averaged winds (Fig. 8). ENSO variability appears as peaks at 25°N and 15°S with a minima near the equator. There are regions of enhanced variability around 75°N, and a broad band of variability from 40° to 70°S for periods greater than 8 months.

The spectra for the observed winds (Fig. 9) shows many similarities to the AMIP spectra. The observed ENSO modulation of the subtropics was moderately stronger in the Northern Hemisphere and was farther south in the Southern Hemisphere. Nevertheless, the subtropics have the same basic structure.

The observed winds showed a very strong LF maxima in the 70°–85°S band (Fig. 9). Neither the AMIP nor NMC10 runs (Fig. 10) suggested a maxima over the Antarctic. Examination of the observed time series showed abrupt changes in the "climatology," which suggests that most of the LF power was from changes in the analysis procedure.

The spectra for NMC10 (Fig. 10) is much weaker than the AMIP spectra and showed a distribution with less frequency dependence. For the most part, the spectral peaks are not statistically significant (white noise hypothesis) except for the peak at 25°N and between 50 and 20 months. This peak suggests that the NMC10 simulation had some internal modes with long timescales.

During the end of 1982 and the beginning of 1983, the AMIP simulation went through an extreme event as illustrated by a four standard deviation anomaly in the 50°–60°S zonal winds (Fig. 11). Obviously this will affect the statistics. A short triangular spike will add, except for the highest frequencies, white noise to the power spectra which is not critical to our analysis. However, the coherence can be affected in more subtle ways. To evaluate the impact of the 1983 event, we have calculated the coherence using both the 1980–92 (Fig. 12) and 1984–92 data (Fig. 13).

The most apparent difference between the figures is that the figure with the longer data record (Fig. 12) appears to be more irregular or noisier. An extreme event will often dominate the statistics, and the 1983 event may dominate the coherence from the longer record. The shorter record, on the other hand, does not include the 1983 event and may be smoother because it is the average of nine more similar years. Because of the differences in the two figures, we will mainly discuss the common features. Other features may appear to be statistically significant; however, we expect the 1983 event to make the statistical tests too liberal.

In Figs. 12 and 13, there are two common bands of high coherence. The 10°–35°N band shows high coherence even for periods as short as 8 months.

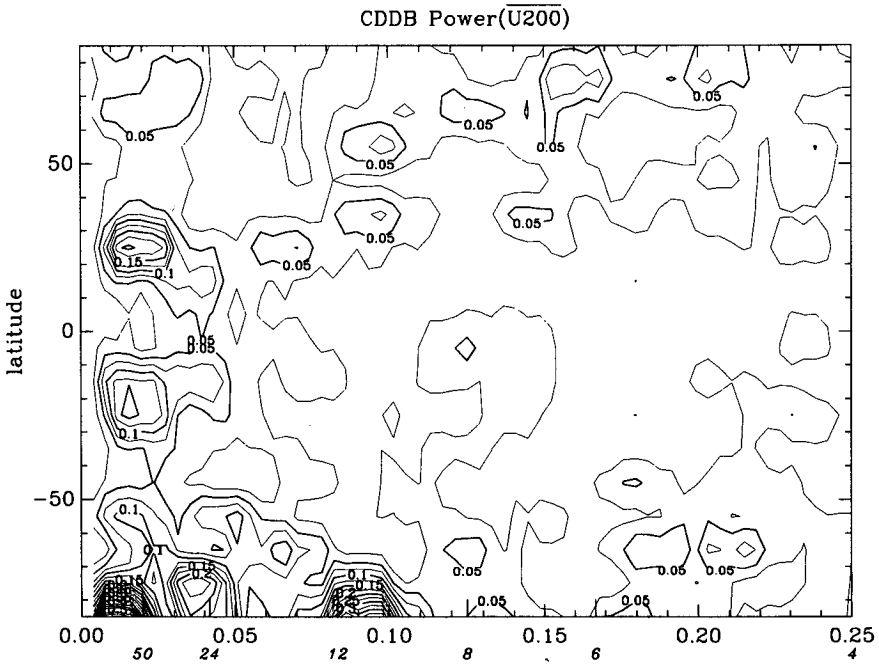

FIG. 9. As in Fig. 8 except observed winds were used.

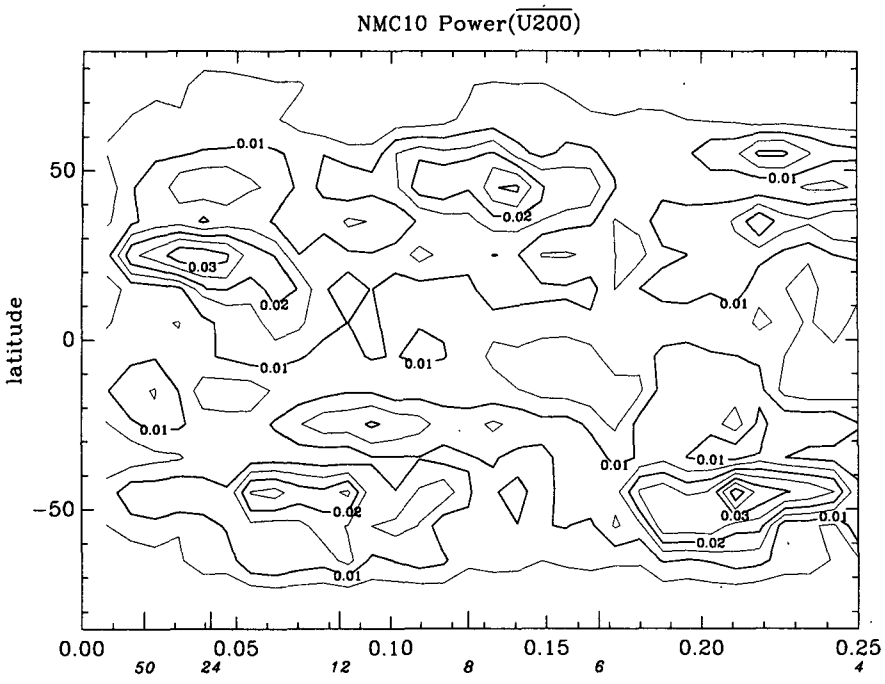

FIG. 10. As in Fig. 8 except NMC10 winds were used.

This band is a region of large LF variability (Fig. 9) and redness in its spectra. The southern subtropical belt (10°–30°S) has lower coherences than the northern belt. In addition, the potential predictability was only found for periods longer 24 months (Fig. 12). Both these latitude bands show strong

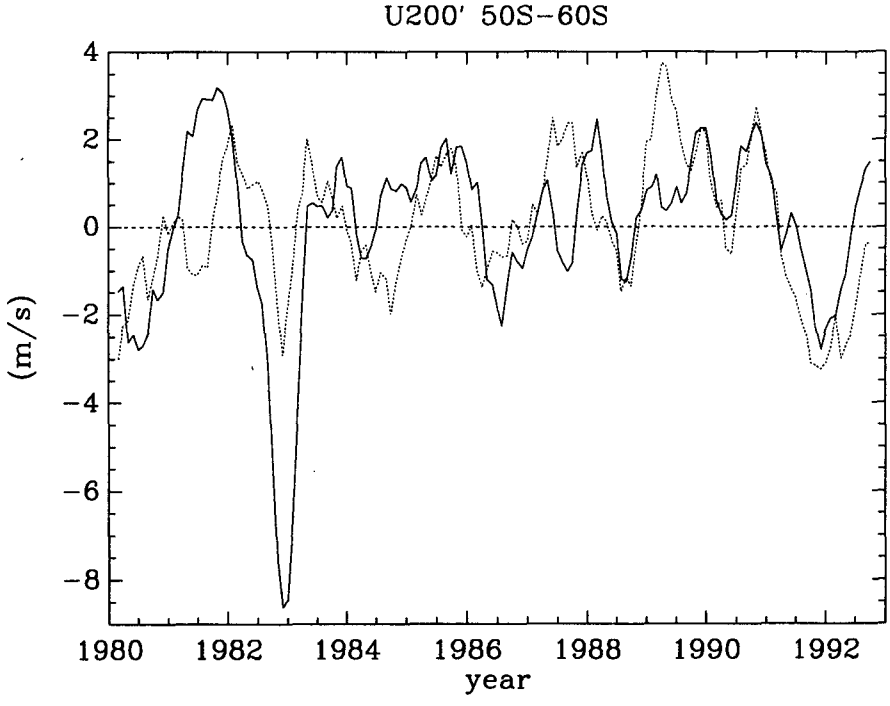

FIG. 11. Five-month running mean of the 200-mb zonal winds averaged in the 50°–60°S latitude belt ($m\ s^{-1}$) for the AMIP simulation (solid line) and observations (dashed line) with the annual cycle removed.

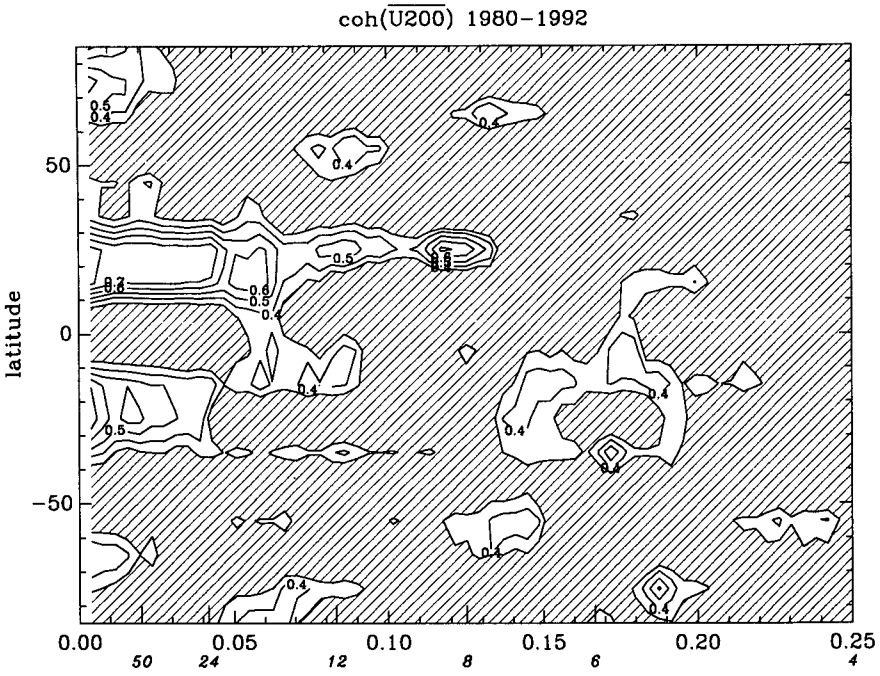

FIG. 12. Coherence of the 200-mb zonal winds from the AMIP simulation and observations for the years 1980–92. The winds were averaged in 10° latitudinal bands before the coherences were calculated. The upper abscissa scale is the frequency in mo^{-1}, and the lower scale is the period in months.

ENSO influences as indicated by the large power at ENSO frequencies.

A narrow band of moderate coherence was found in the southern midlatitudes (50°–60°S) in Fig. 13. While Fig. 12 did not show any significant coherence, the time series (Fig. 11) shows that winds are correlated except for the large deviation, perhaps associated with the 1983 ENSO event. During this event, the AMIP model

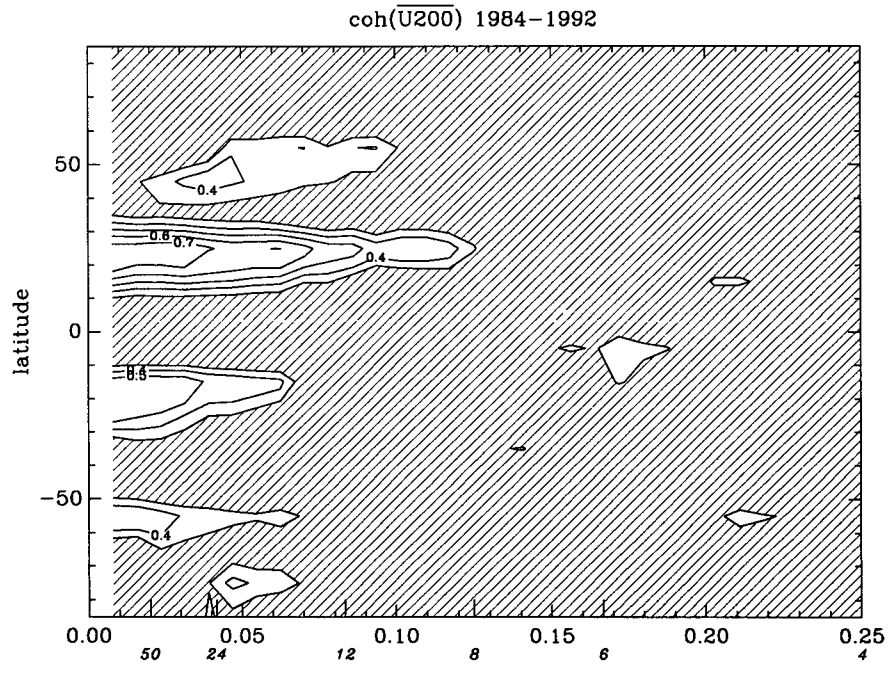

FIG. 13. As in Fig. 12 except only data from 1984 to 1992 were used.

simulated an extreme event, whereas the observed winds suggested a much weaker event. The time series suggests that this latitude band may have a moderate amount of potential predictability. Besides having the hint of potential predictability, the AMIP simulation showed a strong LF maxima in the biennial to ENSO frequency band. The power was up to 25 times larger than in the NMC10 simulation. The observed LF spectrum was also much stronger than the NMC10 spectrum and the white noise level. Thus, the data is very suggestive that this latitude band is strongly affected by the ABC and may have moderate potential predictability in the biennial to ENSO frequency band.

5. Discussion

This investigation of the potential predictability can also be viewed as a diagnostic study on the effects of the boundary conditions in influencing the weather and climate, or as an analysis of the skill of an imperfect atmospheric model coupled with a perfect ocean model. Since a better model or an ensemble of simulations is expected to explain more of the variance, this study should be viewed as being a lower limit.

The NMC10 simulation had low-frequency variability that was approximately white. We hypothesized that the white noise–like spectra was due to synoptic-scale internal variability. If this variability has a timescale on the order of 1 week, then it would appear like white noise to our spectral analysis. If we accept that the white spectra was caused by synoptic-scale internal variability, and this variability is unpredictable at long forecast leads, then the white noise part of the spectrum is unpredictable at long leads.

Fortunately for long-range predictability, ABC can be a strong factor, especially in the LF (Fig. 3). Instead of calculating the potential predictability from the difference of the AMIP and NMC10 simulations (or nature and the NMC10 simulations), we approached the potential predictability as a forecasting problem. We estimated the amount of variance that could be explained (using a modern GCM) given the knowledge of the ABC. This approach avoids the problem of estimating the variance expected in the absence of ABC and the possibility that some of the ABC-related variance may be unpredictable.

Instead of calculating the potential predictability from the spectra, we used the coherence of the AMIP run and observations to estimate the potential predictability. This estimate is specific to a model. However, the estimate is not dependent on any assumptions about the white noise component of the spectra and can be considered a lower bound on the potential predictability. The coherence was found to be a strong function of pressure and latitude. The potential predictability was strongly dictated by the skill in simulating the ENSO effects. This is reasonable as ENSO is connected with the ABC, and ENSO is strongest intradecadal signal in the Tropics. Another important factor in the potential predictability is the magnitude of the ENSO response relative to the internal variability. A perfect ENSO response would be of little predictive value if the internal variability were 100 times larger. Both a good simulation and a strong response to ENSO are necessary conditions for a strong coherence.

The zonal winds had two bands of high potential predictability (Fig. 13). The 15°–25°N band was a region of both strong LF power and significant coherence. At ENSO frequencies, the coherence was approximately 0.75 and remained over 0.4 for periods longer than 8 months. The corresponding Southern Hemisphere band also had high potential predictability. However, the potential predictability was weaker and did not extend to as high frequencies. Besides the two subtropical bands, the 50°–60°S band had suggestions of a moderate potential predictability. Unlike the subtropical bands, this band is not directly affected by the tropical Pacific SST. Perhaps the modulation of the Hadley cell associated with ENSO affected the position and strength of the Southern Hemisphere jet.

Generally, the effects of the ABC were found to be only significant in the very low frequencies (periods longer than 8 months). In addition, the coherences were only significant for certain latitudes and pressure levels. Only the lower frequencies being potentially predictable may be the result of 1) the ABC having more power in the lower frequencies, 2) the lower-frequency ABC being more global in scope, or 3) the adjustment time of the system may be sufficiently long so that a slowly changing forcing is more effective than a higher-frequency forcing of the same amplitude. This bias toward the interseasonal timescale does not imply that there is no monthly variability in the potential predictability. An anomaly may have a timescale of a few years; however, an interaction with the annual cycle may produce higher harmonics. For example, a tropical heating in the Pacific may have a timescale of years; however, this heating could modulate the Pacific–North America pattern (Wallace and Gutzler 1981), which is a seasonal feature. This could result in a response with seasonal or even monthly timescales. Nevertheless, we only found that ABC with an interseasonal timescale had any potentially predictive value (for the variables that we examined).

We found that the coherence was a function of pressure with the strongest coherences in the 200–300-mb levels. Above 100 mb and in the planetary boundary layer, the coherences were very low. Both poor analyses and model deficiencies are to blame. The model also had a weak ENSO response in the lower troposphere. This suggests that model deficiencies may have been responsible for the low coherences at 700 mb.

In summary, we have compared the LF variability of the observed monthly means, and those of two GCM simulations. By comparing a GCM simulation that used observed SST and sea ice with a simulation that used

climatological surface conditions, we found that without ABC, the spectra of the monthly means were usually flat. With ABC, we found large low-frequency peaks superimposed on a white noise spectra. Thus, it appears that ABC are crucially important in forcing the LF variability. In addition, we calculated the coherence between the observations and the GCM run forced by observed SST and sea ice. The effects of the ABC were only apparent in the interseasonal timescales and only for specific latitude bands. The structure in the LF coherence appears related in part to ENSO and to model deficiencies.

Acknowledgments. This work has been supported by the Office of Global Climate Change (NOAA). NMC's AMIP run would not have taken place without the help of Sarah Roy, Harold Lloyd, and Ken Campana, the guidance of Huug van den Dool, and discussions with Hua-Lu Pan, Arun Kumar, Mark Iredell, Ming Ji, Suranjana Saha, Eugenia Kalnay, and Masao Kanamitsu. Reviews by H. van den Dool, R. Livezey, G. White, and the anonymous reviewers are appreciated.

REFERENCES

Chervin, R. M., 1986: Interannual variability and seasonal climate predictability. *J. Atmos. Sci.,* **33,** 233–251.

Dey, C. H., and L. L. Morone, 1985: Evolution of the National Meteorological Center global data assimilation system: January 1982–December 1983. *Mon. Wea. Rev.,* **113,** 304–318.

Ebisuzaki, W., and H. M. van den Dool, 1993: NMC Office Note 402, The Atmospheric Model Intercomparison Project at the National Meteorological Center, 23 pp.

Gates, W. L., 1992: AMIP: The atmospheric model intercomparison project. *Bull. Amer. Meteor. Soc.,* **73,** 1962–1970.

Geleyn, J.-F., M. Rocas, and P. Courtier, 1991: Special features of the unparameterized set of equations for the "ARPEGE" NWP system at DMN. *Proc. of the Ninth Conf. on Numerical Weather Prediction,* Denver, CO, Amer. Meteor. Soc., 231–233.

Lindzen, R. S., and J. R. Holton, 1968: A theory of the quasi-biennial oscillation. *J. Atmos. Sci.,* **25,** 1095–1107.

Lorenz, E. N., 1963: Deterministic nonperiodic flow. *J. Atmos. Sci.,* **20,** 130–141.

——, 1982: Atmospheric predictability experiments with a large numerical model. *Tellus,* **34,** 505–513.

Madden, R. A., 1981: A quantitative approach to long-range prediction. *J. Geophys. Res.,* **86,** 9817–9825.

——, and D. J. Shea, 1978: Estimates of the natural variability of time-averaged temperatures of the United States. *Mon. Wea. Rev.,* **111,** 1696–1703.

Mo, K. C., 1992: The impact of sea surface temperature anomalies on the skill of the seasonal forecasts and northern summer monsoon. *J. Climate,* **5,** 1249–1266.

——, and E. Kalnay, 1991: Impact of sea surface temperature anomalies on the skill of monthly forecasts. *Mon. Wea. Rev.,* **119,** 2771–2793.

Otnes, R. K., and L. Enochson, 1978: *Applied Time Series Analysis,* Vol. 1. *Basic Techniques;* Wiley and Sons, 444 pp.

Qiu, Q.-J., J.-W. Bao, and Q. Xiu, 1991: The significance of mass sink due to precipitation. *Proc. of the Ninth Conf. on Numerical Weather Prediction,* Denver, CO, Amer. Meteor. Soc., 364–365.

Reynolds, R. W., and D. C. Marsico, 1993: An improved real-time global sea surface temperature analysis. *J. Climate,* **6,** 114–119.

Rosen, R. D., and D. A. Salstein, 1983: Variations in atmospheric angular momentum on global and regional scales and the length of the day. *J. Geophys. Res.,* **88,** 5451–5470.

Shea, D. J., and R. A. Madden, 1990: Potential for long-range prediction of monthly mean surface temperatures over North America. *J. Climate,* **3,** 1444–1451.

Van den Dool, H. M., 1994: Long-range weather forecasts through numerical and empirical methods. *Dyn. Atmos. Oceans,* **20,** 247–270.

——, S. Saha, and Z. Toth, 1991: The climate in a multi-year NMC model run. *Proc. of the Fifth Conf. on Climate Variations,* Denver, CO, Amer. Meteor. Soc., 511–514.

Wallace, J. M., and D. S. Gutzler, 1981: Teleconnections in the geopotential height field during the Northern Hemisphere winter. *Mon. Wea. Rev.,* **109,** 784–812.

White, G. H., 1988: Systematic performance of NMC medium-range forecasts 1985–1988. *Proc. of the Eighth Conf. on Numerical Weather Prediction,* Baltimore, MD, Amer. Meteor. Soc., 466–471.

——, and P. M. Caplan, 1991: Systematic performance of the NMC medium-range model. *Proc. of the Ninth Conf. on Numerical Weather Prediction,* Denver, CO, Amer. Meteor. Soc., 511–514.